PAPER • OPEN ACCESS
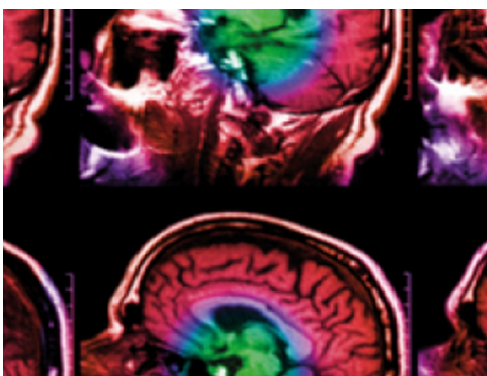
Fitting the determined impedance in the guinea pig inner ear to Randles circuit using square error minimization in the range of 100 Hz to 50 kHz

To cite this article: M O Pleshkov *et al* 2022 *Biomed. Phys. Eng. Express* **8** 025005

View the article online for updates and enhancements.

Biomedical Physics & Engineering Express

Fitting the determined impedance in the guinea pig inner ear to Randles circuit using square error minimization in the range of 100 Hz to 50 kHz

M O Pleshkov[1,2] , S D'Alessandro[3] , M V Svetlik[4], D N Starkov[1,2] , V A Zaitsev[2] , M Handler[3] ,
D Baumgarten[3] , R Saba[5], R van de Berg[1,2] , V P Demkin[2] and H Kingma[1,2]

1   Division of Balance Disorders, Department of Otorhinolaryngology and Head and Neck Surgery, Maastricht University Medical Centre,
    Maastricht, The Netherlands
2   Faculty of Physics, Tomsk State University, Tomsk, Russia
3   Institute of Electrical and Biomedical Engineering, UMIT - Private University for Health Sciences, Medical Informatics and Technology,
    Eduard-Wallnoefer-Zentrum 1, Hall in Tyrol, Austria
4   Biological Institute, Tomsk State University, Tomsk, Russia
5   MED-EL Elektromedizinische Geraete Gesellschaft m.b.H., Innsbruck, Austria

E-mail: maksim.o.pleshkov@gmail.com

Abstract

Objective. Several lumped and distributed parameter models of the inner ear have been proposed to improve vestibular implant stimulation. The models should account for all significant physical phenomena that influence the current propagation, such as the electrical double layer (EDL) and medium polarization. The electrical properties of the medium are reflected in the electrical impedance; therefore, the study aimed to measure the impedance in the guinea pig inner ear and construct its equivalent circuit. *Approach*. The electrical impedance was measured from 100 Hz to 50 kHz between a pair of platinum electrodes immersed in 0.9% NaCl saline solution using sinusoidal voltage signals. The Randles circuit was fitted to the measured impedance in the saline solution in order to estimate the EDL parameters (C, W, and R_{ct}) of the electrode interface in saline. Then, the electrical impedance was measured between all combinations of the electrodes located in the semicircular canal ampullae and the vestibular nerve in the guinea pig *in vitro*. The extended Randles circuit considering the medium polarization (R_i, R_e, C_m) together with EDL parameters (C, R_{ct}) obtained from the saline solution was fitted to the measured impedance of the guinea pig inner ear. The Warburg element was assumed negligible and was not considered in the guinea pig model. *Main results*. For the set-up used, the obtained EDL parameters were: $C = 27.09 \ast 10^{-8} F$, $R_{ct} = 18.75\ k\Omega$. The average values of intra-, extracellular resistances, and membrane capacitance were $R_i = 4.74\ k\Omega$, $R_e = 45.05\ k\Omega$, $C_m = 9.69 \ast 10^{-8}\ F$, respectively. *Significance*. The obtained values of the model parameters can serve as a good estimation of the EDL for modelling work. The EDL, together with medium polarization, plays a significant role in the electrical impedance of the guinea pig inner ear, therefore, they should be considered in electrical conductivity models to increase the credibility of the simulations.

Introduction

The vestibular system—also called the vestibular labyrinth—is a pair of balance organs located in the left and right temporal bones. Each vestibular organ consists of three semicircular canals (SCCs) that detect head angular acceleration and two otolith organs that detect head linear acceleration, including gravity. Head motion information obtained by the vestibular organs is then transferred via nerves to the brain and used to stabilize gaze, facilitate orientation in space, and maintain balance (Kingma and van de Berg 2016). For some reasons, the vestibular function can be decreased or completely lost (Lucieer *et al* 2016),

which significantly worsens the quality of patients' lives and brings a considerable economic burden (Sun *et al* 2014).

Research groups have shown that vestibular function in a population with severe bilateral vestibular loss can be partially restored using an investigational vestibular prosthesis—the vestibular implant (VI) (Perez Fornos *et al* 2017, Boutros *et al* 2019). The concept of the VI is to replace the impaired vestibular end-organ with an electrical stimulator using a set of gyroscopes. Currently, VIs for the semicircular canals consist of three electrode branches, each of which is inserted into one SCC with the stimulating contact targeting the center of the ampulla (van de Berg *et al* 2012, Seppen *et al* 2019). Head rotation is measured by gyroscopes and processed by the VI. Information about head motion is encoded using modulated biphasic charge-balanced square electrical pulses. It is then sent directly into the vestibular nerves through the electrodes - one of each electrode pair being located in the respective SCC, the other located either nearby (bipolar stimulation) or remotely (monopolar stimulation).

In recent years, several distributed parameter models (Hayden *et al* 2012, Marianelli *et al* 2015, Handler *et al* 2017) together with lumped parameter models (Demkin *et al* 2018, 2020) have been proposed for investigation of the current propagation in the tissues of the human and animal inner ear to optimize the VI stimulation. The abovementioned distributed parameter models mainly consider the interelectrode space to be purely resistive. However, medium polarization (Gabriel *et al* 1996a, 1996b) and the electrical double layer (EDL) present in the electrode-tissue interface could influence the shape and amplitude of the voltage waveform (Grant and Lowery 2009). In contrast, lumped parameter models already include the capacitive effects of biological membranes of the cells building up the living tissue.

The EDL represents a small but highly resistive layer at the electrode surface that may influence the current in the range of low frequencies (Cantrell *et al* 2008, Grant and Lowery 2009). In a simplified representation, the EDL can be described as a capacitor preventing the flow of low frequency components of the stimulus. On the other hand, medium polarization (of tissues external to the electrode) can occur at different frequencies. For example, the electronic, ionic, and orientational polarization is present at frequencies higher than the MHz range (gamma dispersion). In contrast, the polarization of cell membranes and macrostructures can arise starting in the range of Hz (alpha dispersion) (Schwan 1957, Grimnes and Martinsen 2010).

The electrical impedance measurements followed by the equivalent circuit fitting approach is widely used in biology studies, including *ex vitro* measurements of isolated animal tissues (Dean *et al* 2008), *in vivo* measurements of plants (Bar-On *et al* 2021), and *ex viv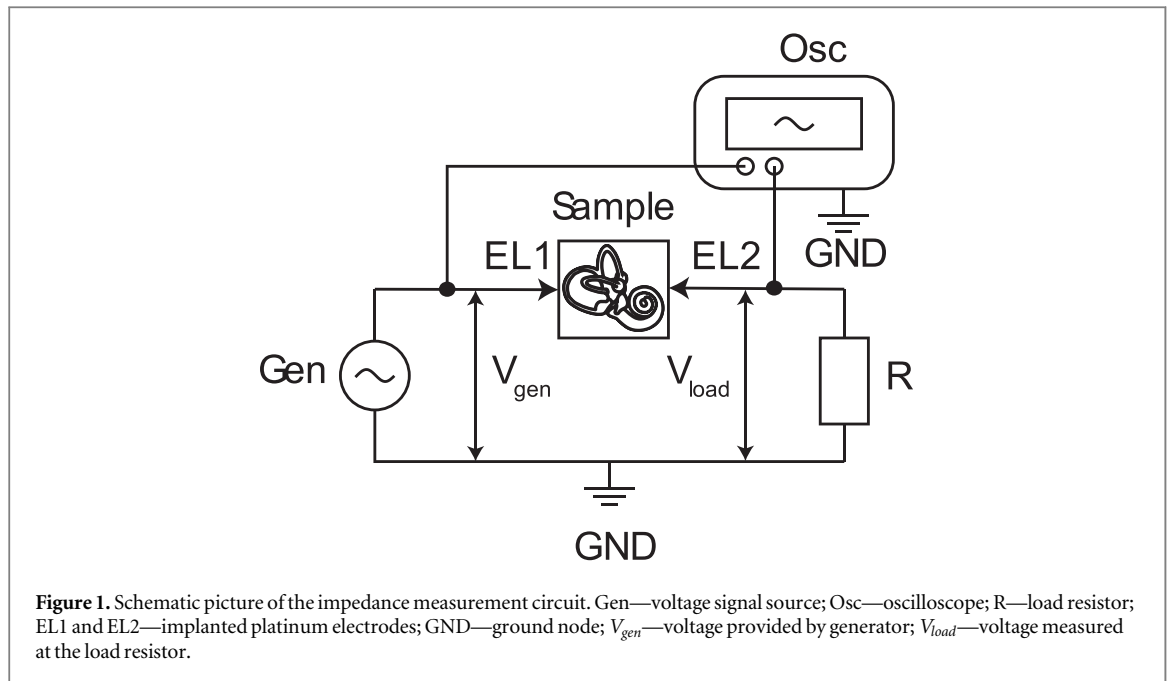o* human dental (Herencsar *et al* 2020) and cardiac (Fischer *et al* 2019) tissues. The most accurate physical models used to optimize the VI should account for all significant physical phenomena of current transmission in the inner ear. Thus, in this study, we performed the following steps: The 0.9% NaCl saline solution was chosen to measure the electrical impedance between a pair of platinum half exposed ball electrodes of 0.5 mm diameter in a frequency range from 100 Hz to 50 kHz. Medium polarization was neglected in this case since the saline solution does not include any tissue and the chosen frequency range is too low to cause gamma dispersion. For this case, the Randles equivalent circuit representing a purely resistive medium and the reactive EDL were the features chosen to fit the measured impedance. Next, the electrical impedances were measured in the guinea pig inner ear between each pair of ampullae and vestibular nerve using the same conditions as in the case of saline solution. All measurements were performed at room temperature T = 298K. Finally, an extended Randles circuit including the reactive component of tissue impedance (instead of purely resistive) and the EDL parameters identified from saline solution measurements were used to fit the measured impedances in the guinea pig.

The first aim of this study was to determine electrical impedances between a pair of electrodes immersed in saline solution to estimate their EDL parameters under such conditions from the fitted Randles circuit. The second aim was to determine electrical impedances between each pair of electrodes, with contacts located close to the center of each ampulla of each SCC and adjacent to the vestibular nerve in the guinea pig inner ear. This was done *in vitro* using sinusoidal voltage signals in a frequency range from 100 Hz to 50 kHz. Finally, the aim was to fit the measured interelectrode electrical impedance, including the EDL and medium polarization, to the Randles circuit using a squared error minimization algorithm.

Materials and methods

Sample

This study used 10 ml of 0.9% NaCl saline solution stored in a disposable plastic container (1.71 × 1.25 × 4.5 cm) and the periotic bone of a guinea pig weighing 947 grams. Before the study, the animal was kept in standard vivarium conditions with water and food *ad libitum*. All procedures were performed following the European Convention for the Protection of Vertebrate Animals. The animal was decapitated under ether anesthesia. The bones of the tympanic cavity and the periotic capsule were removed, with the preserved native structure of the vestibulocochlear nerve leaving this capsule through the internal auditory opening. The study was carried out on a fresh tissue sample no later than an hour after decapitation. The sample was not fixed.

Figure 1. Schematic picture of the impedance measurement circuit. Gen—voltage signal source; Osc—oscilloscope; R—load resistor; EL1 and EL2—implanted platinum electrodes; GND—ground node; V_{gen}—voltage provided by generator; V_{load}—voltage measured at the load resistor.
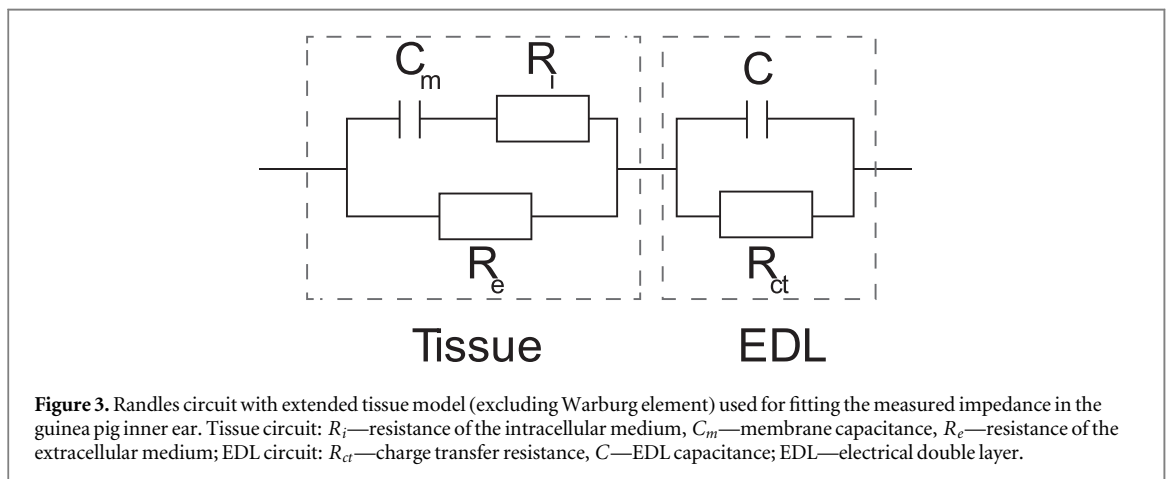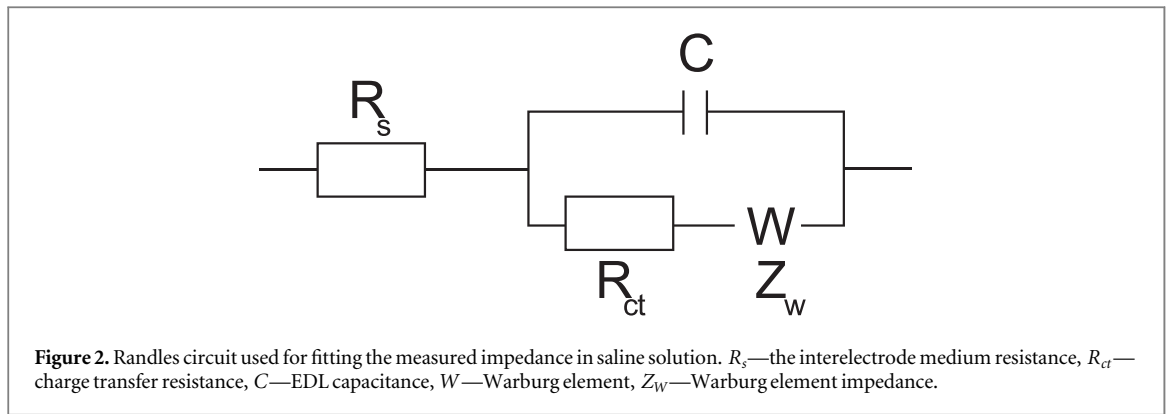
Equipment

A set of platinum electrodes was used to measure the impedances. The platinum ball contact branches fabricated by Med-EL are made by flaming the end of a wire into a ball contact. The size of the ball contact is checked to be within a ± 0.05 *mm* range of tolerance. Each electrode branch was fabricated with a ball contact at the tip with a diameter of 0.5 mm, half exposed, resulting in an estimated contact area of $S_e = \frac{\pi d^2}{2} = 0.39 \ mm^2$. The remaining electrode surface was insulated with silicone rubber. The measured active electrical resistance of each electrode was below $2 \ \Omega$ and thus was considered negligible compared to the EDL. First, two electrodes were inserted parallel to each other in a plastic container filled with 10 ml 0.9% NaCl saline solution, positioned at a distance of 35 mm from each other. Next, three electrodes were each inserted into the fenestrations of one of the three SCC ampullae of the vestibular organ, and one electrode was attached to the vestibulocochlear nerve stump. All electrodes were fixed at their positions using cyanoacrylate (superglue).

The measurement circuit is presented in figure 1. Only two out of four inserted electrodes were used at a time in each of six measurements: one electrode provided the voltage, another served as a ground node. The AC voltage generator (Gen) provided a sinusoidal signal with an amplitude of 0.2 V in the case of saline solution and 0.4 V in guinea pig inner ear, both in a frequency range of 100 Hz to 50 kHz. The chosen magnitude of the load resistor (R) should not interfere with the target impedance. On the other hand, the load resistance should be big enough to register the voltage applied. Thus, in the present study, the load resistor was $R = 960 \ \Omega$ (1% resistance accuracy) for guinea pig measurements and $R = 100 \ \Omega$ (1% resistance

accuracy) for saline solution measurements. During the measurements, the total current flowing in the circuit did not exceed $90 \ \mu A$. The RIGOL DS1054 oscilloscope (Osc) simultaneously registered the voltage applied between the stimulating electrode EL1 and the ground GND (V_{gen}), and the voltage applied between the registering electrode EL2 and the ground GND (V_{load}). The measurements were performed at room temperature T = 298 K.

Electrical impedance calculation

The measurement circuit was considered a closed one (insignificant current flow to and from oscilloscope); therefore, the electrical current was assumed to be the same at any point of the (model) circuit and was determined as $I = \frac{V_{load}}{R}$. Taking into account the previously mentioned assumption and the energy conservation law, the voltage applied to the sample was then calculated simply as a difference between the voltage provided by the generator and the voltage drop over the load resistor: $V_s = V_{gen} - V_{load}$. The electrical impedance magnitude was then calculated at each measured frequency via Ohm's law as the ratio of the voltage and current amplitudes: $|Z(f)| = \frac{|V_s|}{|I|}$. The phase shift $\Delta\varphi = \varphi_2 - \varphi_1$ was determined by comparing the harmonic signal applied from generator $V_{gen} = A_1 sin(\omega t + \varphi_1)$ and the harmonic signal received at the load $V_{load} = A_2 sin(\omega t + \varphi_2)$. Both signals underwent Fast Fourier Transform, then the dominant harmonic component was identified in each signal as having the highest magnitude. The phases φ_1 and φ_2 were calculated in each signal using Euler's formula, and finally, their difference resulted in the overall phase shift $\Delta\varphi$ expressed in radians.

Figure 2. Randles circuit used for fitting the measured impedance in saline solution. R_s—the interelectrode medium resistance, R_{ct}—charge transfer resistance, C—EDL capacitance, W—Warburg element, Z_W—Warburg element impedance.

Figure 3. Randles circuit with extended tissue model (excluding Warburg element) used for fitting the measured impedance in the guinea pig inner ear. Tissue circuit: R_i—resistance of the intracellular medium, C_m—membrane capacitance, R_e—resistance of the extracellular medium; EDL circuit: R_{ct}—charge transfer resistance, C—EDL capacitance; EDL—electrical double layer.

Equivalent circuit model: saline solution

The Randles circuit (Randles 1947) was chosen to simulate the electrical impedance between the electrodes immersed in the saline solution and estimate the EDL parameters since the saline solution does not include any biological tissues or cell membranes. The medium impedance in the saline solution was considered to be purely resistive (R_s) due to the absence of biological tissues in the measurement. The EDL was represented by a capacitor (C) connected in parallel to a Warburg element (W) and an active resistance (R_{ct}) describing the charge transfer through the EDL (figure 2). The Warburg element was represented as a constant phase element with an impedance equal to $Z_W = \frac{1}{A*(i*2*\pi*f)^p}$, where A is the inverse magnitude of Warburg element impedance; i is the imaginary unit, f is linear frequency, and p is a real number in the range between 0 and 1 (Taylor and Gileadi 1995).

Equivalent circuit model: guinea pig inner ear

An extended equivalent Randles circuit was used to fit the measured electrical impedance in the guinea pig inner ear tissue (figure 3). The Randles equivalent circuit was chosen because of the simplicity in its interpretation (impact of the EDL compared with the biological tissue) and lower ambiguity in parameter identification compared with the equivalent circuits incorporating more elements (Demkin *et al* 2020).

The equivalent circuit consists of a simplified EDL circuit without the Warburg element (R_{ct}, C) describing electrode-tissue interface and a tissue circuit representing the inner ear tissue in terms of extracellular resistance (R_e) in parallel with membrane capacitance (C_m) and intracellular resistance (R_i). The Warburg element was omitted due to the small impedance magnitude compared with other resistances and for the simplicity of further simulations. The EDL parameters were taken from the result obtained from the saline solution simulation, whereas the tissue parameters were identified by fitting the tissue circuit to the measured data.

A custom-made algorithm to find the best combination of parameters has been implemented in Matlab 2014b (Mathworks, Natick, USA). The algorithm fitted the desired equivalent circuit to the experimentally determined electrical impedance in the complex form using the iterative method of minimizing the squared error between the fit and the measurements. The initial values of the different parameters and their chosen upper range are listed in table 1; the lower range was always set at 0, since the considered parameters must be non-negative.

Results

Impedance measurements: saline solution

Figure 4 shows the magnitude and phase shift of the total electrical impedance for both measured and fitted
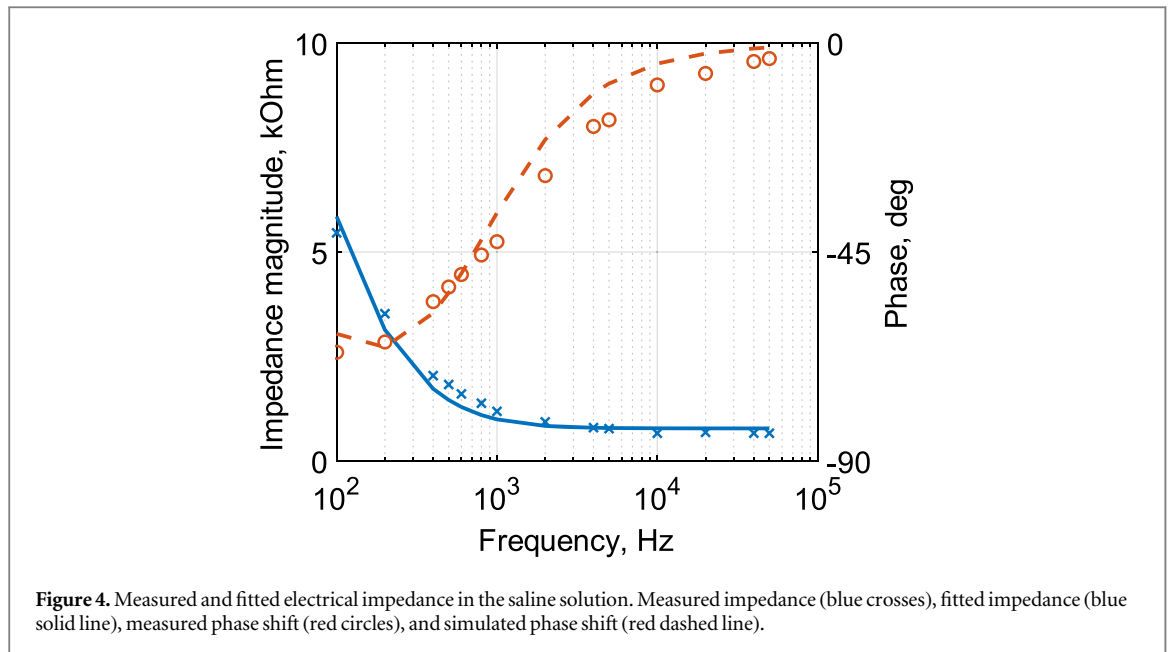
Figure 4. Measured and fitted electrical impedance in the saline solution. Measured impedance (blue crosses), fitted impedance (blue solid line), measured phase shift (red circles), and simulated phase shift (red dashed line).

Table 1. The range of the equivalent circuit parameters used for the model fit.

| | Medium | | | | EDL | | | |
| | Guinea pig tissue | | | Saline | | | | |
	R_i (Ω)	C_m (F)	R_e (Ω)	R_s (Ω)	C (F)	R_{ct} (Ω)	$A\left(\frac{1}{\Omega}\right)$	p
Starting point	$2*10^4$	10^{-9}	$2*10^4$	$2*10^4$	10^{-9}	$4*10^3$	0.06	0.5
Upper limit	10^6	10^{-6}	10^6	10^6	10^{-6}	10^6	Inf	1

Table 2. Fitted parameters of the impedance in the saline solution. R_s—resistance of the interelectrode medium; R_{ct}—charge transfer resistance; C—electrical double layer capacitance; A—the inverse magnitude of Warburg element impedance; p—the power of the phase part of Warburg element impedance.

| | Medium | EDL | | | |
	R_s (Ω)	$C*10^{-8}$ (F)	R_{ct} ($k\Omega$)	$A\left(\frac{1}{\Omega}\right)$	p
saline	809.49	27.09	18.75	0.06	0.89

parameters for the saline solution. The impedance magnitude becomes horizontally asymptotic at approximately 30 kHz with a value of about 1 $k\Omega$. The originally negative phase shift tends to 0 degrees with increasing external field frequency and reaches 0 degrees at around 50 kHz.

Equivalent circuit simulation: saline solution
Table 2 shows the best Randles circuit parameters (figure 2) obtained from the fitting algorithm by using the total measured impedance of the saline solution. The maximum value of Warburg element impedance does not exceed the magnitude of 0.05 Ω and, therefore, can be neglected compared with saline resistance R_s (809.49 Ω) and charge transfer resistance R_{ct} (18.75 $k\Omega$). Thus, the fitted values of EDL (C, R_{ct}) will be used for further simulations of stimulation through real electrodes in the guinea pig inner ear.
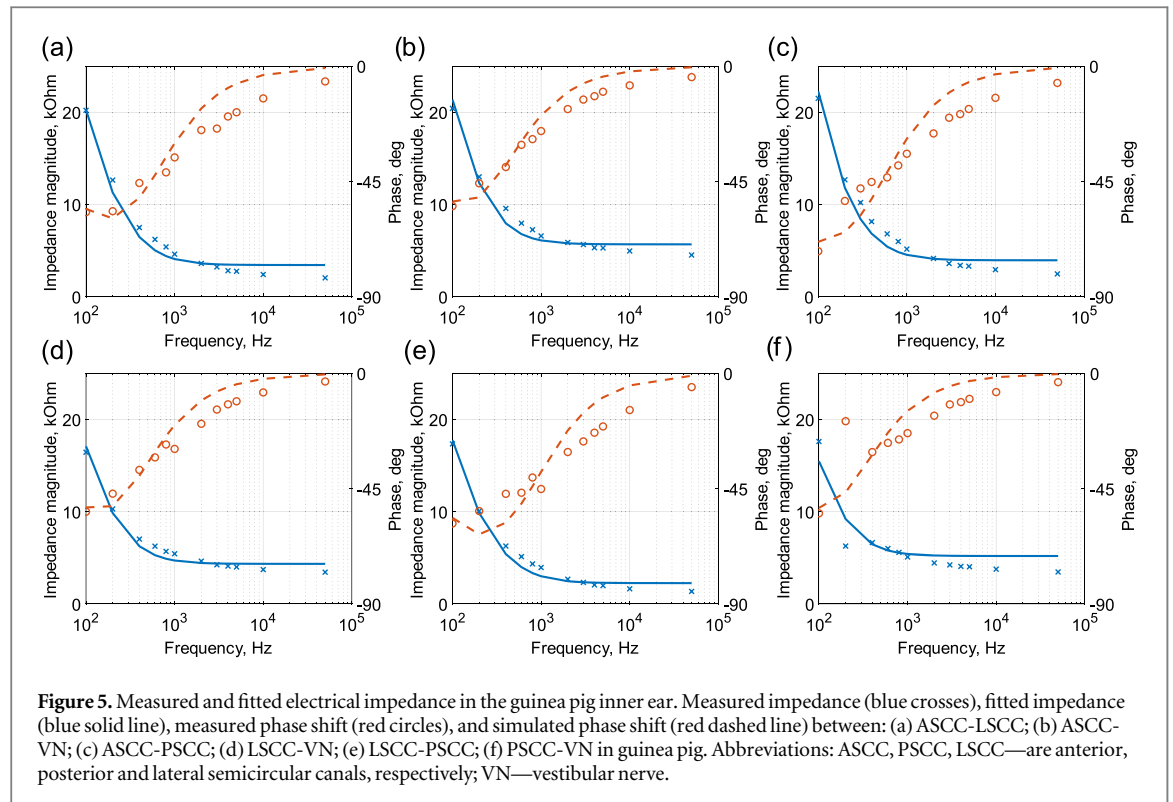
The capacitive impedance (X_C) acts according to the expression $X_C = \frac{1}{i\omega C}$. It forms the low frequency impedance that decays with increasing the stimulation frequency. On the other hand, active resistance of saline (R_s) is frequency independent and determines the plateau value at high frequency range (figure 4).

Impedance measurements: guinea pig
Both measured and fitted magnitudes and phase shifts of a total electrical impedance in the guinea pig inner ear are shown in figure 5. Both the magnitude and phase shift indicate a nonlinear frequency dependence. The measured impedance magnitude becomes horizontally asymptotic at approximately 10 kHz with an average value of 4.6 $k\Omega$. The value of the asymptote also includes the load resistor (960 Ω), which is in series to the measured impedance. The absolute value of phase shift tends to decrease to 0 degrees at approximately the same frequency of 10 kHz.

Equivalent circuit simulation: guinea pig
The extended equivalent Randles circuit was fitted to the measured data to take into account medium polarization, using the circuit shown in figure 3 (including the extended tissue model but without the Warburg element). The other EDL parameters (C and R_{ct}) are defined to be the same as in the saline solution

Figure 5. Measured and fitted electrical impedance in the guinea pig inner ear. Measured impedance (blue crosses), fitted impedance (blue solid line), measured phase shift (red circles), and simulated phase shift (red dashed line) between: (a) ASCC-LSCC; (b) ASCC-VN; (c) ASCC-PSCC; (d) LSCC-VN; (e) LSCC-PSCC; (f) PSCC-VN in guinea pig. Abbreviations: ASCC, PSCC, LSCC—are anterior, posterior and lateral semicircular canals, respectively; VN—vestibular nerve.

Table 3. The fitted impedance parameters in the guinea pig inner ear: Randles circuit with extended tissue. ASCC, PSCC, LSCC—are anterior, posterior, and lateral semicircular canals, respectively; VN—vestibular nerve; R_i—resistance of the intracellular medium; C_m—membrane capacitance; R_e—resistance of the extracellular medium; R_{ct}—resistance of the diffusion layer; C—electrical double layer capacitance; SD—standard deviation. EDL parameters are fixed in this case at levels obtained from the saline solution measurements.

	Medium			EDL	
	R_i $(k\Omega)$	C_m*10^{-8} (F)	R_e $(k\Omega)$	$C*10^{-8}$ (F)	R_{ct} $(k\Omega)$
ASCC-LSCC	3.88	8.44	33.34	27.09	18.75
ASCC-VN	6.76	7.79	35.12		
ASCC-PSCC	4.31	9.50	134.65		
LSCC-VN	5.30	9.94	23.24		
LSCC-PSCC	2.69	9.84	22.86		
PSCC-VN	5.50	12.60	24.08		
Average	*4.74*	*9.69*	*45.05*	—	—
SD	*1.42*	*1.68*	*44.16*	—	—

simulations (table 2). The (small magnitude) Warburg element was not considered in this equivalent circuit since the simulations showed that the absence of the Warburg element does not worsen the goodness of fit. The best fit coefficients are shown in table 3. The fitted intracellular resistance (R_i) between a pair of ampullae is slightly lower than the resistance between an ampulla and the vestibular nerve stump at the location of the recording electrode.

Discussion

In the present study, the electrical impedance was determined in the saline solution and between the selected structures of the guinea pig inner ear: the three SCC ampullae and the vestibular nerve. The

parameters of the Randles circuit were fitted to the measured values of the electrical impedance in the saline solution to estimate the EDL parameters. The obtained magnitude of the Warburg element is considerably smaller than the other elements in the equivalent circuit. Therefore, the Warburg element could be neglected. The extended Randles circuit parameters, including intra- and extracellular resistance and cell membrane capacitance (figure 3) were fitted to the measured electrical impedances in the guinea pig inner ear. A good match between the model and the measurements for both magnitude and phase shift was obtained. A better fit can be obtained by adding more elements in the circuit, but this should be done concerning their physical interpretation.

The data suggest that the capacitive component of the electrical impedance in the guinea pig inner ear is

significant in the range of relatively low frequencies up to 10 kHz. At higher frequencies, the impedance of both capacitors present in the extended Randles circuit approaches zero, allowing the current to bypass the charge transfer resistance and the extracellular resistance and to flow through the intracellular resistance and the membrane capacitance (figure 3). Consequently, the overall magnitude of the electrical impedance approaches (at high frequencies) the total active resistance—equal to the sum of the intracellular resistance and the load resistor with increasing frequency in the model.

The EDL capacitance per unit area can be assumed to be in the range of $\frac{C}{S} = 10 - 20 \frac{\mu F}{cm^2}$ for a metal electrode immersed in liquid (Merrill *et al* 2005), which has the same order of magnitude as the findings of this study $\frac{C}{S} = \frac{C}{2S_e} = 34.73 \ \mu F/cm^2$. The electrode contact area in these experiments is, in fact, twice the area of single contact since the model creates one capacitance value that accounts for the capacitance C for both electrodes; therefore, the direct comparison between literature and fitted values cannot be established.

The equivalent circuit presented in this study can be extended by adding more elements, as suggested by (Demkin *et al* 2020). It will probably allow reaching a better fit; nevertheless, adding more components to the models increases the variability in the parameter values that might lead to model overfitting and the complexity of model interpretation. Therefore, this approach should be treated with caution. We assume that the goodness of fit of the model presented in this study (figure 3) and more complex models will be comparable since all significant physical phenomena contributing to the electrical impedance were taken into account in this study.

In vivo versus in vitro
It has been shown in the literature that there are differences between *in vitro* and *in vivo* results, indicating a slight decrease in the conductivity and permittivity in *in vitro* cases (Schwartz and Mealing 1985). Even though the ionic composition of endo- and perilymphatic liquids equalizes *post mortem* due to the diffusion process (Rodgers *et al* 1966), it does not change the overall liquid conductivity and active resistance R_e. Finally, the tissue properties can change with temperature (Edd *et al* 2005, Fischer *et al* 2019), with the trend to increase when lowering the temperature in the positive temperature range. Thus, the measured impedance evaluated in this paper could be a slight overestimation of the real *in vivo* situation.

It is known that various tissues present between measuring electrodes contribute to the value of electrical impedance (Kauppinen *et al* 1998). In this study, the guinea pig inner ear was removed from the original environment leaving out the surrounding tissues - the brain, muscles, and skin. This might slightly change the measured impedance even though the current is mainly flowing between the measuring electrodes in the key structures (endo- and perilymphatic liquids, vestibular nerve, and temporal bone that are present in the sample) as it would happen in *in vivo* measurements. Eventually, similar impedance measurements can potentially be performed in animals *in vivo* if the proper surgical approach is applied.

Relation to a human inner ear
When considering the human inner ear space, the value of the EDL capacitance will probably vary from the findings of this study due to the bigger sizes of vestibular labyrinths (in particular, of the SCCs and the ampullae). Electrode dimensions used in humans can be bigger or smaller than in the *in-vitro* experiments of this study on guinea pigs. This might lead to different contact surface areas and, consequently, different EDL capacitances - C, which in its way affects the impedance in the low frequency range. The electrode size issue can be resolved in each particular case by direct measurement of the implant electrode tip and a consecutive scaling the EDL capacitance.

In addition, the human ampullae are located farther from each other and from the vestibular nerve than in the guinea pig, which will probably increase the active resistance - R_e. On the other hand, the cross-sections of human semicircular canals are approximately 20 times bigger than in the guinea pig (Curthoys *et al* 1977) that will probably reduce the active resistance - R_e according to the cylinder resistance equation (if the canal can be assumed as a conductive cylinder).

This study presents the electrical impedances not only between each pair of ampullae but also between the ampullae and vestibular nerve, which is crucial to understand the nerve fiber stimulation processes and cross-talk between stimulated ampullae. The presented methodology to evaluate fitting parameters by matching the measured *in vitro* electroconductive properties of the guinea pig inner ear could improve modelling the electrode-tissue interface and evaluate simulations. The obtained values of the EDL parameters (C, W, R_{ct}) can serve as a good estimate of the EDL to use in future electrical modelling, including other electrode dimensions, even though they might change with different electrode contact areas. Unlike the EDL, the medium impedance would change with different interelectrode distances and tissues present between the electrodes, such as bone, membrane, or cupula. Eventually, the physical phenomena described in this article remain the same for guinea pig and human inner ear can be used for modeling purposes.

Future prospective
In the future, *in vivo* experiments measuring the interelectrode impedance in laboratory animals (and

potentially in VI patients) will be very useful for validating the presented results.

A (micro-) Computed Tomography scan of the implanted site after impedance measurements would allow for the reconstruction of the entire geometry and determine the precise distance between electrodes located in the inner ear. Together with the obtained impedances in the inner ear, the known geometry would allow for the construction of 3D FEM models and calculation of the distributed parameters such as electrical conductivity and dielectric permittivity of the tissues involved (Fischer *et al* 2019).

The measured electrical impedances of the guinea pig inner ear and obtained equivalent circuits shown in this study can also be used to improve and optimize already existing 3D FEM models by considering the EDL in the simulations. In addition, impedance measurements from various isolated tissues of the inner ear and identification of their distributed electrical parameters might be essential to get more realistic localized results from the 3D FEM simulations.

Conclusion

The EDL, together with medium polarization, plays a significant role in the electrical impedance of the guinea pig inner ear. Thus, when trying to predict the performance of electrical stimulation using electrical conductivity models, the EDL and medium polarization should be considered in these models to increase the credibility of the simulation outcomes.

Acknowledgments

Data availability statement

The data that support the findings of this study are available upon reasonable request from the authors.

Ethical statement

All procedures performed in studies involving animals were in accordance with the ethical standards of the institution at which the studies were conducted and ethical approval was obtained from the Bioethics Committee of the Institute of Biology at Tomsk State University, registration No34, minute No18 dated December 2, 2019.

ORCID iDs

M O Pleshkov ⓘ https://orcid.org/0000-0002-4131-0115
S D'Alessandro ⓘ https://orcid.org/0000-0002-6134-8532
D N Starkov ⓘ https://orcid.org/0000-0001-8703-4008
V A Zaitsev ⓘ https://orcid.org/0000-0002-5303-5309
M Handler ⓘ https://orcid.org/0000-0001-7958-3162
D Baumgarten ⓘ https://orcid.org/0000-0001-6109-3368
R van de Berg ⓘ https://orcid.org/0000-0001-9734-8668
V P Demkin ⓘ https://orcid.org/0000-0002-2183-5811
H Kingma ⓘ https://orcid.org/0000-0001-9880-8224

References

Grant P F and Lowery M M 2009 Effects of the electrical double layer and dispersive tissue properties in a volume conduction model of deep brain stimulation *Proceedings of the 31st Annual International Conference of the IEEE Engineering in Medicine and Biology Society: Engineering the Future of Biomedicine, EMBC 2009* 6497–500

Bar-On L, Garlando U, Sophocleous M, Jog A, Motto Ros P, Sade N, Avni A, Shacham-Diamand Y and Demarchi D 2021 Electrical modelling of in-vivo impedance spectroscopy of nicotiana tabacum *Plants Front. Electron.* **0** 14

Boutros P J *et al* 2019 Continuous vestibular implant stimulation partially restores eye-stabilizing reflexes *JCI Insight* **4** 1–19

Cantrell D R, Inayat S, Taflove A, Ruoff R S and Troy J B 2008 Incorporation of the electrode-electrolyte interface into finite-element models of metal microelectrodes *J. Neural Eng.* **5** 54–67

Curthoys I S, Markham C H and Curthoys E J 1977 Semicircular duct and ampulla dimensions in cat, guinea pig and man *J. Morphol.* **151** 17–34

Dean D A, Ramanathan T, Machado D and Sundararajan R 2008 Electrical impedance spectroscopy study of biological tissues *J. Electrostat.* **66** 165

Demkin V P, Kingma G, Mel'nichuk S V, Svetlik M V, Rudenko T V, Akinina M D and Suyundukova A T 2020 Effect of leakage currents on the formation of electrical pulse for the vestibular nerve stimulation *Russ. Phys. J.* **62** 2228–34

Demkin V P, Shchetinin P P, Melnichuk S V, Kingma H, Van de Berg R, Pleshkov M O and Starkov D N 2018 Electric current transmission through tissues of the vestibular labyrinth of a patient: perfection of the vestibular implant *Russ. Phys. J.* **60** 2019–24

Edd J F, Horowitz L and Rubinsky B 2005 Temperature dependence of tissue impedivity in electrical impedance tomography of cryosurgery *IEEE Trans. Biomed. Eng.* **52** 695–701

Fischer G, Handler M, Johnston P R and Baumgarten D 2019 Impedance and conductivity of bovine myocardium during freezing and thawing at slow rates - implications for cardiac cryo–ablation: Impedance of bovine myocardium during freezing and thawing *Med. Eng. Phys.* **74** 89–98

Gabriel C, Gabriel S and Corthout E 1996a The dielectric properties of biological tissues: I. literature survey *Phys. Med. Biol.* **41** 2231–49

Gabriel S, Lau R W and Gabriel C 1996b The dielectric properties of biological tissues: II. measurements in the frequency range 10 Hz to 20 GHz *Phys. Med. Biol.* **41** 2251–69

Grimnes S and Martinsen Ø G 2010 Alpha-dispersion in human tissue *J. Phys. Conf. Ser.* **224** 012073

Handler M, Schier P P, Fritscher K D, Raudaschl P, Chacko L J, Glueckert R, Saba R, Schubert R, Baumgarten D and Baumgartner C 2017 Model-based vestibular afferent stimulation: Modular workflow for analyzing stimulation

scenarios in patient specific and statistical vestibular anatomy *Front. Neurosci.* **11** 713

Hayden R, Sawyer S, Frey E, Mori S, Migliaccio A A and Della Santina C C 2012 Virtual Labyrinth model of vestibular afferent excitation via implanted electrodes—Validation and application to design of a multichannel vestibular prosthesis *Exp. brain Res.* **210** 623–40

Herencsar N, Freeborn T J, Kartci A and Cicekoglu O 2020 A Comparative study of two fractional-order equivalent electrical circuits for modeling the electrical impedance of dental tissues *Entropy* **22** 1–19

Kauppinen P K, Hyttinen J A and Malmivuo J A 1998 Sensitivity distributions of impedance cardiography using band and spot electrodes analyzed by a three-dimensional computer model *Ann. Biomed. Eng.* **26** 694–702

Kingma H and van de Berg R 2016 Anatomy, physiology, and physics of the peripheral vestibular system *Handbook of Clinical Neurology* **137** 1–16

Lucieer F, Vonk P, Guinand N, Stokroos R, Kingma H and van de Berg R 2016 Bilateral vestibular hypofunction: Insights in etiologies, clinical subtypes, and diagnostics *Front. Neurol.* **7** 26

Marianelli P, Capogrosso M, Luciani L B, Panarese A, Bassi Luciani L, Panarese A and Micera S 2015 A computational framework for electrical stimulation of vestibular nerve *IEEE Trans. Neural Syst. Rehabil. Eng.* **23** 897–909

Merrill D R, Bikson M and Jefferys J G R 2005 Electrical stimulation of excitable tissue: Design of efficacious and safe protocols *J. Neurosci. Methods* **141** 171–98

Perez Fornos A, Cavuscens S, Ranieri M, van de Berg R, Stokroos R, Kingma H, Guyot J-P and Guinand N 2017 The vestibular implant: A probe in orbit around the human balance system *J. Vestib. Res.* **27** 51–61

Randles J E B 1947 Kinetics of rapid electrode reactions *Discuss. Faraday Soc.* **1** 11–9

Rodgers K, Chou J T and Rodgers B K 1966 Concentrations of inorganic ions in guinea-pig inner ear fluids. II. Post-mortem changes in the ionic composition of utricular endolymph and perilymph *J. Laryngol. Otol.* **80** 885–9

Schwan H P 1957 *Electrical properties of tissue and cell suspensions* 5 (New York: Academic) (https://doi.org/10.1016/b978-1-4832-3111-2.50008-0)

Schwartz J L and Mealing G A R 1985 Dielectric properties of frog tissues *in vivo* and *in vitro Phys. Med. Biol.* **30** 117–24

Seppen B F *et al* 2019 Drafting a surgical procedure using a computational anatomy driven approach for precise, robust, and safe vestibular neuroprosthesis placement-when one size does not fit all *Otol. Neurotol.* **40** S51–8

Sun D Q, Ward B K, Semenov Y R, Carey J P and Della Santina C C 2014 Bilateral vestibular deficiency: quality of life and economic implications *JAMA Otolaryngol. Head Neck Surg.* **140** 527–34

Taylor S R and Gileadi E 1995 Physical interpretation of the warburg impedance *Corrosion* **51** 664–71

van de Berg R, Guinand N, Guyot J-P, Kingma H and Stokroos R J 2012 The modified ampullar approach for vestibular implant surgery: feasibility and its first application in a human with a long-term vestibular loss *Front. Neurol.* **3** 18